THE JOURNAL OF PHYSICAL CHEMISTRY LETTERS
A JOURNAL OF THE AMERICAN CHEMICAL SOCIETY

pubs.acs.org/JPCL
Letter

Which Ion Dominates the Temperature and Pressure Response of Halide Perovskites and Elpasolites?

Loreta A. Muscarella,*[,‖] Huygen J. Jöbsis,[‖] Bettina Baumgartner, P. Tim Prins, D. Nicolette Maaskant, Andrei V. Petukhov, Dmitry Chernyshov, Charles J. McMonagle, and Eline M. Hutter*

Cite This: J. Phys. Chem. Lett. 2023, 14, 9042−9051
Read Online

ACCESS | Metrics & More | Article Recommendations | Supporting Information

ABSTRACT: Halide perovskites and elpasolites are key for optoelectronic applications due to their exceptional performance and adaptability. However, understanding their crucial elastic properties for synthesis and device operation remains limited. We performed temperature- and pressure-dependent synchrotron-based powder X-ray diffraction at low pressures (ambient to 0.06 GPa) to investigate their elastic properties in their ambient-pressure crystal structure. We found common trends in bulk modulus and thermal expansivity, with an increased halide ionic radius (Cl to Br to I) resulting in greater softness, higher compressibility, and thermal expansivity in both materials. The A cation has a minor effect, and mixed-halide compositions show intermediate properties. Notably, thermal phase transitions in $MAPbI_3$ and $CsPbCl_3$ induced lattice softening and negative expansivity for specific crystal axes, even at temperatures far from the transition point. These results emphasize the significance of considering temperature-dependent elastic properties, which can significantly impact device stability and performance during manufacturing or temperature sweeps.

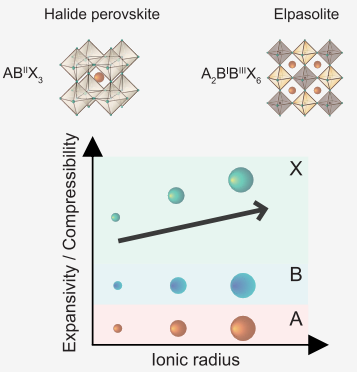

Lead halide perovskite and related lead-free elpasolite (i.e., double perovskite) semiconductors are widely investigated for a variety of optoelectronic applications, including photovoltaics,[1−4] light-emitting diodes,[5,6] photoredox catalysis,[7−10] and radiation detection.[11−13] The unprecedented interest in this class of materials can be understood from its excellent optoelectronic performance in combination with enormous chemical and structural flexibility. For instance, mixing halides in lead halide perovskites enables the absorption onset and emission wavelength over the entire visible range of the light spectrum to be tuned.[14] In halide elpasolites, with the general formula $A_2B^IB^{III}X_6$, bandgap tunability can be obtained by mixing metals at the B^{III} site, such as Bi, Sb, In, or Fe,[15−17] and to some extent by mixing halides (X site).[18−20] In contrast to the plethora of studies of optoelectronic properties and applications of halide perovskites and elpasolites, there is still limited knowledge about their mechanical properties, such as compressibility and expansivity, and how these properties vary with the temperature and crystal axis. The solution-processed deposition of halide perovskites and elpasolites in the form of thin films onto substrates involves increased temperatures ranging from 100 to 200 °C. Additionally, the differences in the structural and thermal properties of substrates and halide perovskites, such as lattice parameters and thermal expansion coefficients, can lead to strain and deformations during thin film deposition. Previously, we and others have found that compression slows halide migration and that compression or strain can activate or suppress light-induced halide segregation.[21−24] Thus, quantifying the extent to which this class of relatively soft materials responds to changes in temperature and pressure leading to stress-induced deformations is key for growing stable thin films of these perovskites and manipulating their optoelectronic properties. Previous studies that report on elastic properties used diamond anvil cells (DACs) to apply external pressure[23,25−31] and hence probed high-pressure regimes (several to hundreds of gigapascals) and crystal phases that are far from relevant to their ambient crystal structure. The deformations induced in halide perovskite films during the solution-processed deposition are comparable to the exertion of mild pressure (<0.5 GPa).[32] Therefore, hydraulic pressure techniques are needed to investigate how the crystal structure would respond in a more relevant pressure range. Given that the typical annealing temperatures applied during the deposition of halide perovskite thin films (100 °C) yield film stress levels of <0.06 GPa,[32] our work, conducted through synchrotron-based powder X-ray diffraction (XRD), explored the structural properties of halide perovskites and elpasolites at increased pressures of ≤0.060 GPa, using a hydrostatic pressure cell. Importantly, this allowed us to determine the elastic properties of the materials in their crystal structures relevant to ambient conditions. The pressure-dependent measurements were performed between room temperature

Received: August 28, 2023
Accepted: September 27, 2023
Published: October 2, 2023

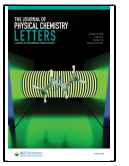

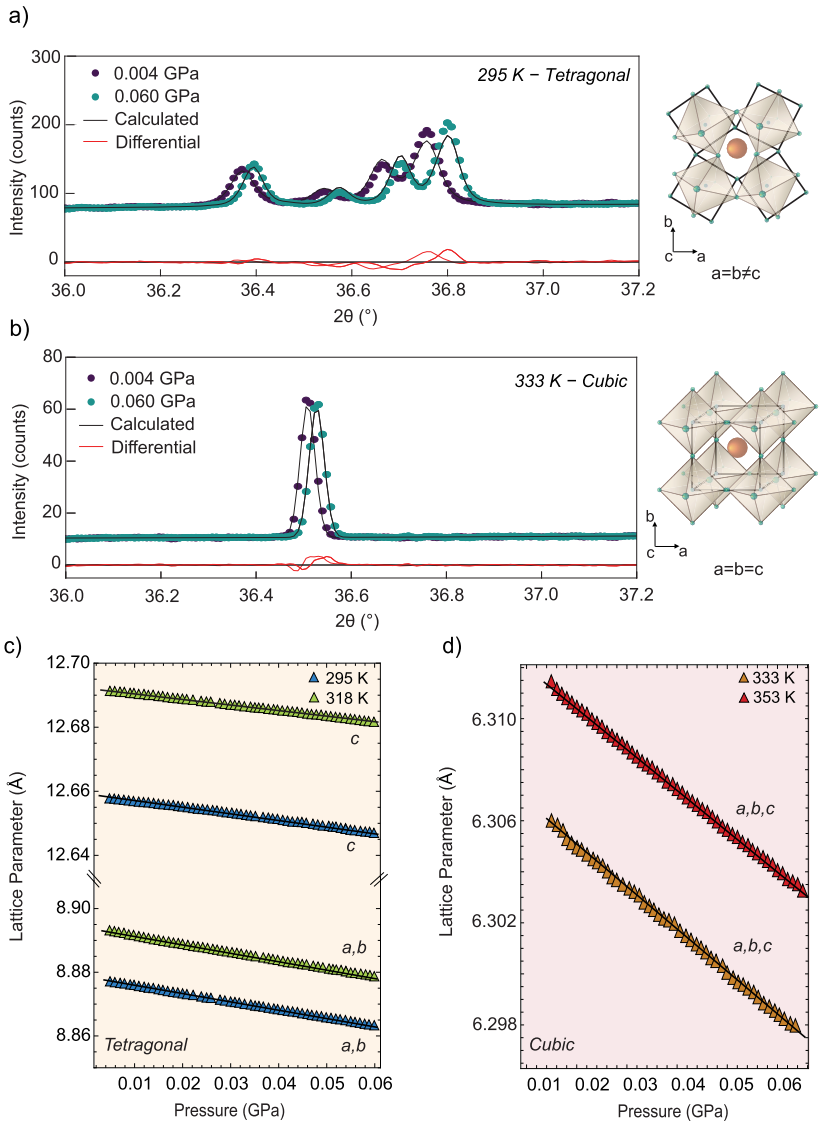

Figure 1. Selected reflections of the diffraction pattern of $MAPbI_3$ collected at (a) room temperature and (b) 333 K, at 0.004 (purple) and 0.060 GPa (green), together with schematic drawings of the crystal structures. The calculated profile structure is colored black, and the residuals of the fit are colored red. Pressure-dependent lattice parameters of (c) tetragonal $MAPbI_3$ (*I*4/*mcm* space group)[39] collected at 295 and 318 K and (d) cubic $MAPbI_3$ ($Pm\bar{3}m$ space group) collected at 335 and 355 K obtained from refinements using the Rietveld method. Fits are shown as black solid lines.

and 90 °C (298−363 K), a typical temperature range for thin film synthesis and photovoltaic operation conditions. We report the temperature-dependent bulk modulus for a wide variety of compositions, including $MAPbCl_3$, -Br_3, and -I_3 (MA = methylammonium), mixed-halide variants thereof, $CsPbCl_3$, -Br_3, and -I_3, and the elpasolites $Cs_2AgBiCl_6$ and -Br_6 and mixed-halide and trivalent metal variants thereof. These materials were synthesized as powders using mechanochemical synthesis in a ball, which has been successfully used to make both perovskite and elpasolite materials.[10,33−36] Powders are employed as a model system because they do not experience strain from the substrate. By using the same fabrication and measurement approach for a large number of compositions, we exclude effects from sample type or varying the synthesis procedure used in different laboratories, enabling us to draw robust and general conclusions about the fundamental properties and behaviors of these materials. Hence, we find some general trends in the elastic properties of halide perovskites and elpasolites. For all perovskite and elpasolite materials, we find that the iodide-based materials are substantially softer than their bromide- and chloride-based analogues and that the bulk modulus increases from I^- to Br^- to Cl^-. The mixed-halide perovskites show bulk moduli between those of their pure compounds and, within the same crystal phase, exhibit a linear relation with the average halide radius. In addition, the bulk modulus appears to be constant in the investigated temperature range for all materials, provided that the materials remain in the same crystal structure. For both $CsPbCl_3$ and $MAPbI_3$, which undergo phase transitions at ∼325 and ∼330 K, respectively, we observe a decrease in the bulk modulus at temperatures close to the phase transition. In addition, as the elastic properties of noncubic perovskites are anisotropic, we also estimate the compressibility in different crystallographic directions. Finally, we find that some temperature-dependent phase transitions of halide perovskites are reflected in negative thermal expansion coefficients of certain crystal axes, already several tens of degrees below the transition temperature. The variation of thermal expansivity with a crystal

https://doi.org/10.1021/acs.jpclett.3c02403
J. Phys. Chem. Lett. 2023, 14, 9042−9051

axis (for noncubic perovskites) and crystal structure (i.e., temperature) could induce stress during synthesis or temperature cycling and, in turn affect the stability of the corresponding devices (e.g., ion migration). For instance, elpasolites are used in scintillation detectors, which convert high-energy radiation (such as γ rays) into visible light, allowing for their detection. By incorporating the knowledge of elastic properties, researchers can design elpasolite-based detectors that are more mechanically stable, ensuring a consistent performance over time in harsh environments. Additionally, the knowledge of the elastic properties can help identify potential phase transitions or structural instabilities in both lead halide perovskites and elpasolites, guiding researchers in avoiding conditions that might lead to undesirable changes in the crystal structure. Therefore, elastic properties should be considered for thin films in the design of optoelectronic devices of halide perovskites.

Microcrystalline powder samples of $MAPb(Cl_{1-x}Br_x)_3$, $MAPb(I_{1-x}Br_x)_3$, $CsPbCl_3$, -Br_3, and -I_3, and several elpasolites (based on Cl^-, Br^-, Bi^{3+} and/or Fe^{3+}, Sb^{3+}, or In^{3+}) were made via mechanochemical synthesis in a ball mill,[10,33−36] as described in the Experimental Section in the Supporting Information. To quantify the effect of both pressure and temperature on the structural parameters of these halide perovskites and elpasolites, we performed pressure- and temperature-dependent powder XRD measurements using a synchrotron radiation source at European Synchrotron Radiation Facility (ESRF) beamline BM01.[37] We used a hydrostatic pressure cell filled with a fluorinated inert liquid (FC-770) as a pressure-transmitting medium, and we performed pressure sweeps from 0.004 to 0.060 GPa at temperatures of 298, 318, 335, and 355 K. Additional details of the experimental setup can be found in the Experimental Section in the Supporting Information. This approach enables one to directly measure the variation of structural parameters as a function of pressure and temperature and thereby allows one to determine material properties such as the bulk modulus (B), compressibility (K), and thermal expansivity (α). Figure 1a shows selected reflections of the diffraction pattern of tetragonal ($I4/mcm$ space group) $MAPbI_3$ collected at 0.004 and 0.060 GPa and room temperature. The external compression shifts the diffraction peaks to larger 2θ values, while the crystal phase remains constant in the range of pressures explored. Figure 1b shows the diffraction pattern of $MAPbI_3$ collected at 333 K. At this temperature, $MAPbI_3$ is in a cubic crystal structure ($Pm\bar{3}m$ space group). Also in this case, we observe the shift of the reflections toward larger 2θ values without an indication of phase transition induced by external pressure. In panels c and d of Figure 1, we plot the lattice parameters of tetragonal $MAPbI_3$ [room temperature, where $a = b \neq c$ (Figure 1c)] and cubic $MAPbI_3$ [333 K, where $a = b = c$ (Figure 1d)] as a function of external pressure. This pressure-induced variation of the lattice parameters was determined from refinements using the Rietveld method using FullProf Suite;[38] i.e., the obtained diffractograms were fitted using pseudo-Voigt functions considering the unit cell dimensions and atomic coordinates as variables. Further details of the method are provided in the Experimental Section in the Supporting Information. In all cases, as expected, applying external pressure leads to a decrease in the lattice parameter.

To investigate the role of the halide on the temperature-dependent elastic properties, we have performed a similar analysis of the mixed-halide perovskites $MAPb(Cl_{1-x}Br_x)_3$ and $MAPb(I_{1-x}Br_x)_3$, as reported in Figures S1−S7. Except for $MAPbI_3$, which has tetragonal ($I4/mcm$ space group) symmetry in the range of 298−330 K,[40,41] these perovskites show cubic symmetry ($Pm\bar{3}m$ space group) under these conditions.[23,42] For all single- and mixed-halide perovskites, we observed a linear decrease in volume with pressure for the temperatures explored. The isothermal equation of state for a solid is given by bulk modulus B:

$$B = \frac{\text{pressure}}{\text{strain}} = -\frac{\Delta P}{\Delta V}V \quad (1)$$

where $\Delta P/\Delta V$ is the derivative of pressure with respect to volume and V the volume at ambient pressure. By fitting this function to the pressure−volume trends (Figures S1 and S7), we estimated the bulk moduli (B) of the single halide (iodide, bromide, and chloride) and mixed-halide series $MAPb(Cl_{1-x}Br_x)_3$ and $MAPb(I_{1-x}Br_x)_3$. The results are shown in Figure 2a and listed in Table S1. In the entire temperature range of 298−355 K, $MAPbBr_3$ (halide fraction $x = 1$) has a bulk modulus of 17 GPa, which gradually increases upon replacement of the Br^- with Cl^-. An increase in the bulk modulus is associated with an increase in the stiffness of the material. At room temperature, $MAPbCl_3$ has a bulk modulus of 20 GPa, which seems to be slightly lower (19 GPa) at increased temperatures. However, over the entire temperature range, the bromide-based perovskites are significantly softer than the perovskites containing chloride. The introduction of iodide leads to further softening of the perovskites, gradually decreasing the bulk modulus to 14 GPa. This softening of the bulk modulus with larger halides is consistent with previous single-crystal studies reporting a smaller Young's modulus of the {100} crystal facet.[43]

For the cubic systems, we observe a linear relation between the bulk modulus and the average halide radius as common for metal alloys (Figure S8).[44] Such findings confirm previous assumptions with similar compositions[21] but are in contrast with theoretical predictions for $CsPb(I_{1-x}Br_x)_3$.[45] To investigate the role of the MA^+ cation in the halide perovskite and the role of the trivalent metal in the elpasolite structure with respect to their elastic properties, we determined the temperature-dependent bulk moduli of $CsPbBr_3$ and -Cl_3, as well as bulk moduli of $Cs_2AgBiBr_6$ and -Cl_6 and $Cs_2AgInCl_6$. The results are shown in panels b and c of Figure 2 and Figures S9−S13, and numeric values are listed in Table S1. Even though the Cs-based perovskites have crystal structures different from the MA-based ones, the room-temperature bulk moduli of $CsPbBr_3$ [B = 17.5 GPa (see Figure S12)] and $CsPbCl_3$ [B = 19 GPa (see Figure 2c and Figure S13)] are almost identical to those of their MA-based counterparts (i.e., <1 GPa variation). These observations suggest that the mechanical properties are mostly defined by the framework of corner-sharing PbI_3 (Cl_3 or Br_3) octahedra. Upon examination of Pb−X bonding from a perspective of electronegativity (EN), the EN values of X gradually decrease from chlorine to iodine (i.e., 3.16 for Cl > 2.96 for Br > 2.66 for I according to the Pauling scale). With a constant EN for Pb (1.87), the nature of bonding shifts from being primarily ionic for Cl to more covalent for I.[46] Ionic compounds tend to possess hardness and brittleness, while covalent compounds lean toward softness and flexibility, which is reflected in the values of bulk moduli and compressibility we found in this study. A similar trend is observed upon comparison of the bromide- to chloride-based elpasolites. Also, the stiffer nature

https://doi.org/10.1021/acs.jpclett.3c02403
J. Phys. Chem. Lett. 2023, 14, 9042−9051

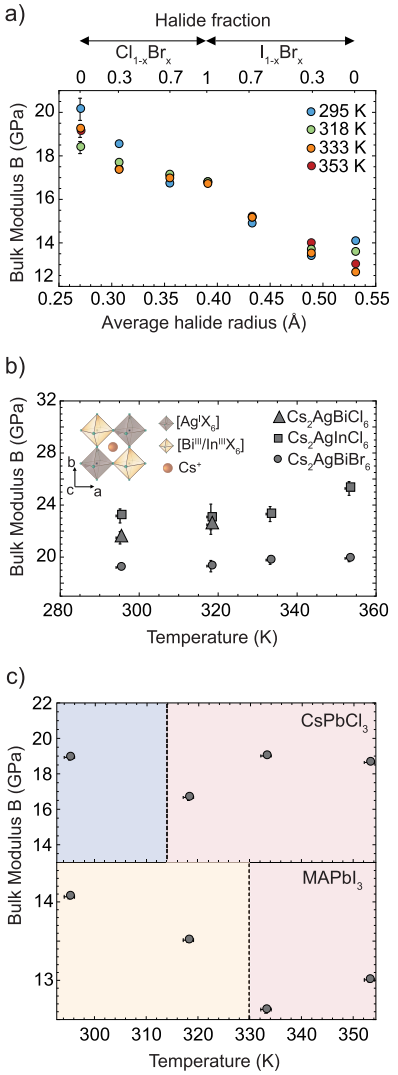

Figure 2. (a) Bulk moduli (B) of methylammonium (MA) lead mixed-halide perovskites as a function of the average halide radius and the mixing halide (Cl, left; Br, middle; I, right) ratio at 295, 318, 335, and 355 K. This shows that the Cl-based materials soften upon addition of Br^- and that I^- leads to further softening of the lattice. Note that except for $MAPbI_3$, all of these perovskites exhibit a cubic symmetry, and their bulk modulus is roughly constant with temperature. (B) Bulk moduli of halide double perovskites $Cs_2AgBiBr_6$ (circles), $Cs_2AgInBr_6$ (squares), and $Cs_2AgBiCl_6$ (triangles) as a function of temperature. Also here, the Cl-based compounds are stiffer than $Cs_2AgBiBr_6$, with only minor temperature effects. All of the compositions are in the cubic phase, and no phase transition is observed. (C) Bulk moduli of $MAPbI_3$ and $CsPbCl_3$ as a function of temperature. The blue, yellow, and red regions correspond to the orthorhombic, tetragonal, and cubic phases, respectively. The dashed lines correspond to the temperature at which the phase transition occurs.

of the In−Cl elpasolites compared to Bi−Cl elpasolites could be due to its more ionic behavior arising from larger EN difference with the chloride (i.e., 1.78 for In vs 2.02 for Bi). Comparing the perovskites to the elpasolites, we observe that the replacement of Pb^{2+} with both Ag^+ and a trivalent cation (Bi^{3+} or In^{3+}) leads to a stiffening of the lattice, associated with larger bulk moduli, i.e., 22−23 GPa for those with Cl^- and 19 GPa for $Cs_2AgBiBr_6$,[27] even though the Ag−X and Bi−X bonds are expected to be less ionic than the Pb−X bonds on the basis of their EN. Comprehending the full trend that encompasses alterations of metal, halide, and crystal structure therefore necessitates further investigation. However, overall, the effect of changing the cations is relatively small compared to the effect of changing the halides, so that the halide framework dominates the mechanical properties of halide perovskites and elpasolites rather than the A or B site cations. Interestingly, the elpasolite compositions exhibit bulk moduli on par with those of metal−organic framework (MOF) perovskites, such as $[(CH_3)_2NH_2][M(HCOO)_3]$, where M = Mn^{2+}, Fe^{2+}, or Cu^{2+} (with bulk moduli ranging from 24 to 27 GPa[47]). Hence, the halide perovskites and elpasolites investigated in this study demonstrate bulk moduli significantly lower than those of other materials with similar structures, such as $KCuF_3$ (B = 57 GPa[48]), $LaMnO_3$ (B = 108 GPa[49]), and La_2NiMnO_6 (B = 179 GPa[50]). This renders them notably more susceptible to strain and external pressure in contrast to other materials.

Another general finding obtained from our study is that most of the bulk moduli only slightly change with temperature in the range from 298 to 355 K, in contrast with the expected decrease in B with temperature observed in oxide perovskites, and the expected increase calculated for tin-based halide perovskites such as $CsSnI_3$.[51] As one can see in panels a and b of Figure 2, the variation of the bulk modulus with the halide is larger than any temperature effect in this range. Two notable exceptions include $CsPbCl_3$ and $MAPbI_3$, which undergo temperature-dependent phase transitions between 298 and 330 K, shown in Figure 2c. Our data hint toward a softening of the materials (i.e., lower bulk modulus) close to their transition temperature (dotted lines). This finding is particularly relevant because temperature-dependent elastic properties may introduce stress during fabrication of halide perovskite and elpasolite thin films or during temperature cycling processes in operating devices.

Considering that the bulk modulus is a volume property, while the elastic properties of noncubic perovskites, such as tetragonal $MAPbI_3$, are in general anisotropic and therefore depend on crystallographic direction, we derived the compressibility of the specific crystal axes by monitoring their compression as a function of applied pressure (e.g., K_a, for compressibility along the a-axis):

$$K_a = -\frac{a_f - a_0}{a_f}P \tag{2}$$

where a is the lattice parameter and $a_f - a_0$ the change in lattice parameter between the lattice parameter at the final (a_f) and initial (a_0) pressures. Hence, we determined the compressibility for the a-, b-, and c-axes for noncubic perovskites. The volumetric compressibility, K_V, i.e., the susceptibility of a material to compress upon external applied pressure, is inversely proportional to B and is calculated as reported in Supporting Note 2, and the values are listed in Table S5. The compressibilities along the a-, b-, and c-axes for the compositions studied are reported in Tables S2−S4. Figure 3 shows that compression along the a- and b-axes of tetragonal $MAPbI_3$ and orthorhombic $CsPbCl_3$ is significantly larger than that for the c-axis. In addition, we observe that the compressibility of c increases significantly in $CsPbCl_3$ during the orthorhombic-to-cubic phase transition as well as in $MAPbI_3$ during the tetragonal-to-cubic phase transition, as it becomes identical to those of the a- and b-axes. In orthorhombic $CsPbBr_3$, we find that compression along the

https://doi.org/10.1021/acs.jpclett.3c02403
J. Phys. Chem. Lett. 2023, 14, 9042−9051

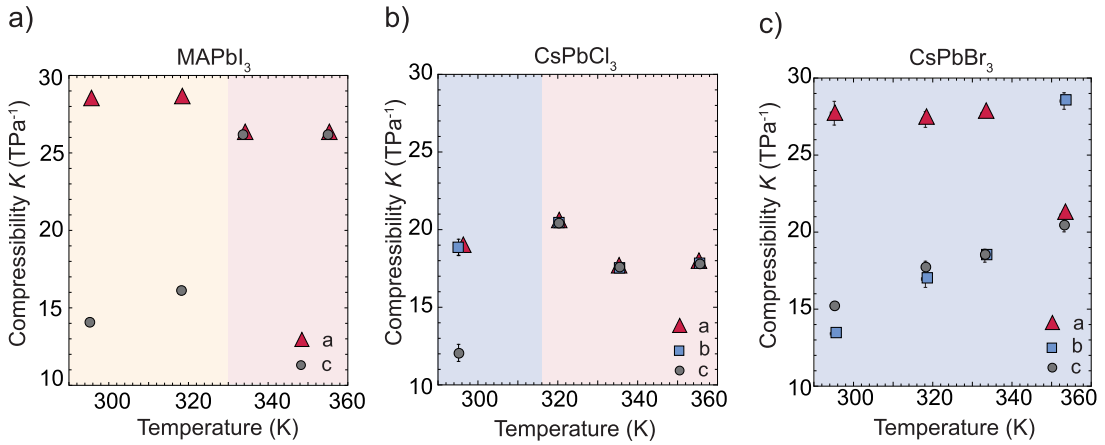

Figure 3. (a) Compressibility K of the crystal axes in the tetragonal (yellow) and cubic (red) phases of $MAPbI_3$. The compressibility of the c-axis is smaller than that of the a-axis in the tetragonal phase. (b) Compressibility K of the crystal axes in the orthorhombic (blue) and cubic (red) phases of $CsPbCl_3$. The compressibility of the c-axis is smaller than those of the a- and b-axes in the orthorhombic phase. (c) Compressibility K of the crystal axes in the orthorhombic (blue) phase. The compressibility of the b-axis is smaller than those of the a- and c-axes in the tetragonal phase up to 353 K where an abrupt change is observed. At 353 K, the compressibility of the b-axis is larger than those of the a- and c-axes. Error bars are, in some cases, smaller than the data point size.

a- and c-axes is significantly larger than that for the b-axis. Additional pressure studies using an extended temperature range are needed to determine the origin of the observed axis-dependent compressibility. For $CsPbBr_3$, we observe a gradual increase in the compressibility of the b- and c-axes with temperature, in combination with swapping of the compressibility of the a- and b-axes at 353 K. This phenomenon may occur in the case of an anti-isostructural phase transition,[52,53] although more measurements are needed to conclusively show whether such a transition exists in $CsPbBr_3$. To investigate the relation between the pressure response and thermal expansivity, we further measured the temperature-dependent XRD of single-halide perovskites ($MAPbI_3$, $MAPbBr_3$, $MAPbCl_3$, $CsPbBr_3$, and $CsPbCl_3$) and elpasolites ($Cs_2AgBiBr_6$, $Cs_2AgBiCl_6$, and $Cs_2AgInCl_6$) between 100 and 400 K. A similar Rietveld refinement was used to study the temperature dependence of a-, b-, and c-axes. The results are shown in Figure 4, whereas the lattice parameters reported in pseudocubic notation are reported in Figure S14. Here, blue areas represent orthorhombic ($Pnmb$ space group), yellow areas tetragonal ($I4/mcm$ space group), and red areas cubic symmetry ($Pm\bar{3}m$ space group). Although similar experiments have been reported for a selection of these compositions,[40,42,54,55] we here compare the thermal expansivities of all compositions using identical synthesis and measurement conditions and link the thermal response to the elastic properties of the same materials.

Comparing the different halide perovskites and elpasolites in cubic symmetry (red areas), we observe an increase in lattice parameters as a function of temperature, associated with a positive thermal expansivity, as shown in Table 1. In line with the halide-dependent trend in bulk modulus, for all compositions studied here the thermal expansivity is observed to increase in the following order due to the softness of the material: Cl < Br < I. We observe that the elpasolites are less expandable with temperature than the lead halide perovskites, with thermal expansivities of 2.86×10^{-5} K^{-1} for $Cs_2AgBiBr_6$ and 2.42×10^{-5} K^{-1} for $Cs_2AgBiCl_6$. This observation is consistent with their larger bulk moduli, showing that the elpasolite structure is more resistant to changes in both temperature and pressure. Furthermore, the absolute values are close to recent theoretical predictions.[56] Note that previous studies of $Cs_2AgBiBr_6$ thin films have reported a cubic-to-tetragonal phase transition at 122 K.[57] The absence of this phase transition (at least down to 100 K) for the mechanochemically synthesized powders studied here may be related to differences in strain between the powders and thin films. Note that $Cs_2AgBiBr_6$ stands out as the sole exception; the other compositions exhibit the expected phase transitions at their respective temperatures.

Additional lab-based temperature-dependent XRD on elpasolite with mixed trivalent metals, i.e., $Cs_2Ag(Bi_{0.5}Sb_{0.5})Br_6$, $Cs_2Ag(Bi_{0.5}In_{0.5})Br_6$, and $Cs_2Ag(Bi_{0.9}Fe_{0.1})Br_6$, and mixed halides such as $Cs_2AgBi(Br_{0.33}I_{0.67})_6$ (Supporting Note 4 and Figures S20 and S21) indicates higher thermal expansivity for elpasolites containing I^- ions, identical to the lead-based perovskites (see Table 1). Previous work already showed a minor role of the Cs cation on the thermal expansivity in halide elpasolites,[58] and we here also find that the metal cation does not affect the thermal expansivity. For phases with symmetry lower than cubic, i.e., orthorhombic (blue) and tetragonal (yellow), thermal expansivity is anisotropic. Interestingly, the axis-dependent thermal expansivity and compressibility in the tetragonal crystal structure follow the same trend (i.e., the c-axis is less expandable and more compressible than the a- and b-axes). On the contrary, in the orthorhombic crystal phase we observe no such relation, suggesting that thermal expansivity and compressibility are decoupled in this phase. An additional consideration is that some lattice parameters have nonlinear temperature-dependent thermal expansivity. For example, the axes of orthorhombic $CsPbBr_3$ and $CsPbCl_3$ and tetragonal $MAPbI_3$ show a nonlinear dependence of lattice parameter with temperature, so that the thermal expansivity becomes temperature-dependent (see Supporting Note 3 and Table S6). Notably, in all halide perovskites studied here, the c-axis of the tetragonal phase has a negative thermal expansivity in at least part of the temperature range. According to Landau theory, such a behavior reflects bi-linear coupling of the order parameter and spontaneous lattice strain.[59] Considering that negative thermal expansivity values (i.e., thermal contraction) are mainly observed at temperatures "close" to thermal phase transitions, it seems likely that these two phenomena are

https://doi.org/10.1021/acs.jpclett.3c02403
J. Phys. Chem. Lett. 2023, 14, 9042−9051

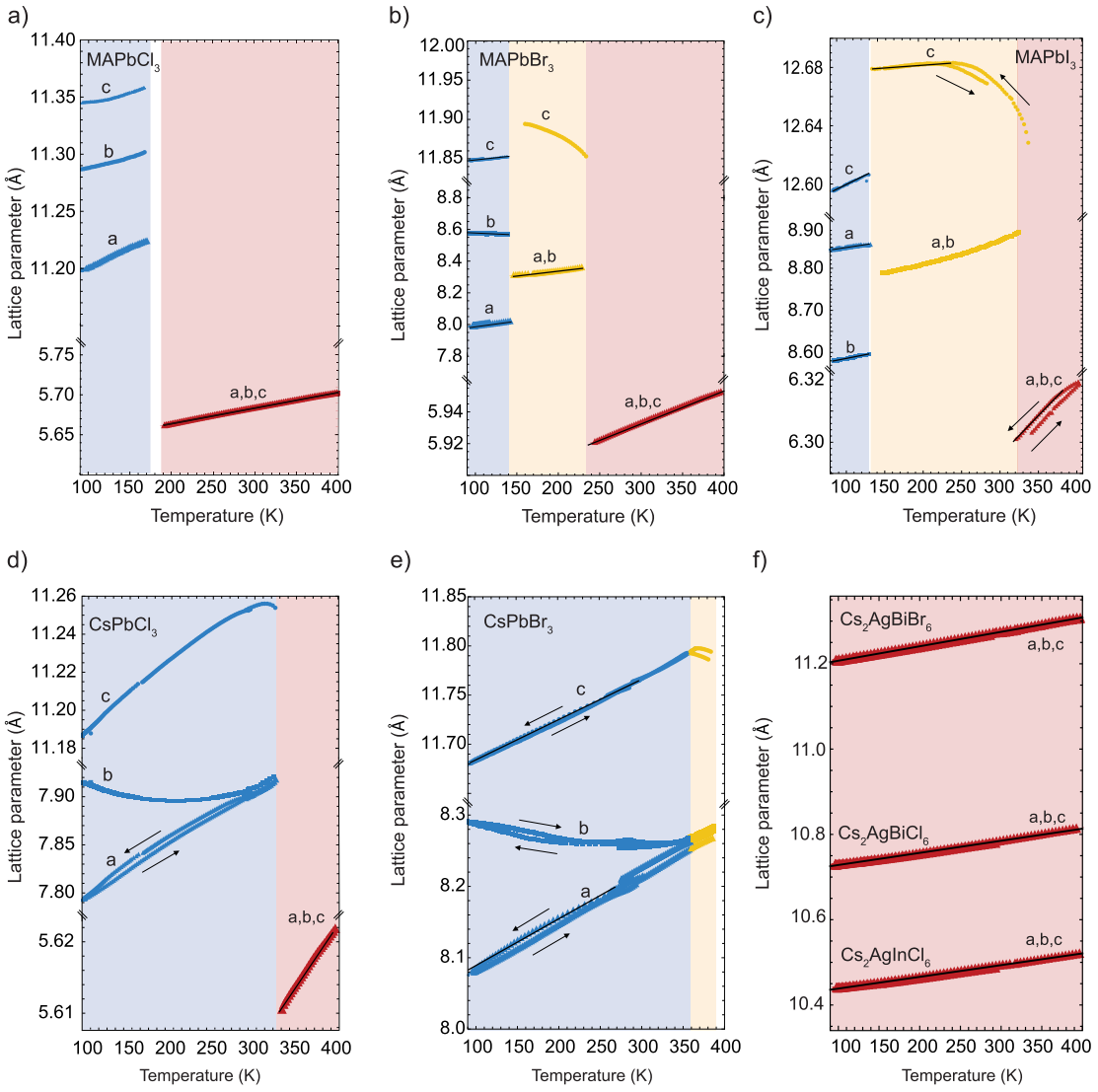

Figure 4. Temperature-dependent lattice parameters of (a) $MAPbCl_3$, (b) $MAPbBr_3$, (c) $MAPbI_3$, (d) $CsPbCl_3$, (e) $CsPbBr_3$, and (f) $Cs_2AgBiBr_6$, $Cs_2AgBiCl_6$, and $Cs_2AgInCl_6$ obtained from profile Rietveld refinement of synchrotron XRD patterns collected between 90 and 400 K. The blue, yellow, and red regions correspond to the orthorhombic, tetragonal, and cubic phases, respectively. The white regions correspond to the temperature range in which two phases coexist in the XRD patterns. The black arrows indicate the direction of temperature variation, i.e., cooling (arrow down) and heating (arrow up). Solid lines represent the fits for the linear thermal expansivity.

related. Previous work has reported similar behavior for $MAPbI_3$ and formamidinium lead iodide ($FAPbI_3$) perovskites[60−62] as well as several oxide-based materials that undergo phase transitions.[63] For $CsPbBr_3$ and $CsPbCl_3$, the temperature range with negative thermal expansivity for the *c*-axis is relatively small (20−40 K). In contrast, for $MAPbBr_3$ and $MAPbI_3$, the negative thermal expansivity of the *c*-axis is already observed 100 K below the tetragonal−cubic phase transition. This observation, together with temperature-dependent bulk modulus from Figure 2a, shows that the range in which the phase transition is affecting thermal and elastic properties is substantially broader than previously thought on the basis of the (much smaller) temperature range in which crystal phases coexist.[40] This has major implications for synthesizing thin films on substrates with thermal expansivities different from those exhibited by the perovskite, where the temperature gradient during cooling from annealing to room temperature will introduce strain into the material.

We determined temperature-dependent elastic properties of several halide perovskites (namely, single and mixed halide) and elpasolite (namely, mixed halides and mixed trivalent metals) from pressure- and temperature-dependent diffraction experiments using a synchrotron radiation source. We used temperatures ranging from 298 to 363 K (i.e., ambient to 90 °C), which is a typical temperature range for thin film synthesis and photovoltaic operation conditions. To obtain information relevant to ambient phases, we explored pressures from ambient to 0.06 GPa. We find that the elastic properties and the thermal expansivity in both halide perovskites and elpasolites are dominated by the halide framework, with lower bulk moduli for larger halide radius size (Cl < Br < I). It is worth noting that in both lead halide perovskites and elpasolites, the elastic properties are intimately connected with the type of bond formed between the metal and the halide. As the halide undergoes a transition from the more electronegative Cl^- to the less electronegative I^-, the bonding characteristics evolve from being predominantly ionic to

https://doi.org/10.1021/acs.jpclett.3c02403
J. Phys. Chem. Lett. 2023, 14, 9042−9051

Table 1. Thermal Expansivities along All Crystal Axes for All Compositions[a]

	orthorhombic ($\times 10^{-5}$ K^{-1})		tetragonal ($\times 10^{-5}$ K^{-1})		cubic ($\times 10^{-5}$ K^{-1})
$MAPbI_3$	a	3.81	$a = b$	function[b]	4.04
	b	2.02			
	c	5.81	c	0.34	
$MAPbBr_3$	a	9.04	$a = b$	6.99	3.53
	b	−2.79			
	c	1.00	c	function[b]	
$MAPbCl_3$	a	function[b]	–		3.51
	b	function[b]			
	c	function[b]			
$CsPbBr_3$	a	7.68	–		3.27[c]
	b	function[b]			
	c	3.51			
$CsPbCl_3$	a	function[b]	–		3.02
	b	function[b]			
	c	function[b]			
$Cs_2AgBi(Br_{0.33}I_{0.67})_6$	–		–		5.08[c]
$Cs_2AgBiBr_6$	–		–		2.86
$Cs_2AgBiCl_6$	–		–		2.42
$Cs_2AgInCl_6$	–		–		2.49
$Cs_2Ag(Bi_{0.5}In_{0.5})Br_6$	–		–		2.84[c]
$Cs_2Ag(Bi_{0.5}Sb_{0.5})Br_6$	–		–		3.34[c]
$Cs_2Ag(Bi_{0.9}Fe_{0.1})Br_6$	–		–		3.16[c]

[a]If the temperature response is nonlinear, the experimental data are fitted using a second-order polynomial and denoted by "function". The optimized parameters of these fits are given in Supporting Note 3 and Figures S15−S19. As the temperature range in which the materials are orthorhombic, tetragonal, or cubic varies with composition, the reported (functions of) thermal expansivity is valid only in that specific temperature range. [b]Nonlinear expansivity (see Supporting Note 3). [c]Data collected with a lab-based X-ray diffractometer.

becoming increasingly covalent. This shift influences the behaviors of the materials. Ionic compounds often exhibit traits of hardness and brittleness, whereas covalent compounds tend to demonstrate qualities of softness and flexibility. These inherent properties are effectively mirrored in the bulk moduli and compressibility values, as found in our research. On the contrary, the monovalent cation and the trivalent metal have a minor role in determining elastic properties. The bulk modulus of these materials remains constant within the investigated temperature range provided that the crystal structure remains unchanged. On the contrary, we observe that thermal phase transitions lead to a decrease in the bulk modulus (i.e., softening of the material), as exemplified by $MAPbI_3$ and $CsPbCl_3$. For noncubic systems, in which the elastic properties are anisotropic, we obtained axis-dependent compressibility. Our results suggest that the c-axis is much harder than the a- and b-axes in tetragonal $MAPbI_3$ and orthorhombic $CsPbCl_3$, whereas the b-axis is the hardest axis in $CsPbBr_3$. Furthermore, we find that some temperature-dependent phase transitions of halide perovskites are accompanied by negative thermal expansivity of certain crystal axes, already several tens of degrees below the phase transition temperature. This observation shows that the range in which the phase transition is affecting thermal and elastic properties is substantially broader than previously thought on the basis of the (much smaller) temperature range in which phases coexist. Altogether, these findings have major implications for synthesizing thin films at substrates with thermal expansivities different from those of the perovskite and elpasolite, where the temperature gradient during the synthesis and the temperature cycling during device operation will introduce strain into the material, consequently exerting a noteworthy influence on the functionality of related devices. Hence, acquiring a deep comprehension of the temperature-dependent elastic properties in these materials is essential for bolstering the advancements in strain engineering that has proven to be a potent tool for manipulating both the optical properties and the stability of perovskite thin films.

■ ASSOCIATED CONTENT

Data Availability Statement

Data and fit procedures reported in this study can be accessed at https://data.esrf.fr/doi/10.15151/ESRF-ES-1022932247 (raw data) and https://data.esrf.fr/doi/10.24416/UU01-W60H58 (processed data) and are available under a CC-BY Creative Commons Attribution 4.0 International license.

Supporting Information

The Supporting Information is available free of charge at https://pubs.acs.org/doi/10.1021/acs.jpclett.3c02403.

Experimental details, materials, and methods; lattice parameters as a function of pressure, $P-V$ curves, temperature-dependent bulk moduli, and axis-dependent compressibility for all of the compositions explored; *in situ* temperature-dependent XRD of several elpasolites; tables of temperature-dependent bulk moduli, axis-dependent compressibility, and temperature-dependent expansivity; lab-based temperature-dependent X-ray diffraction for additional elpasolites; calculation of volumetric and axis-dependent thermal expansivity and compressibility; and calculation of the bulk moduli (PDF)

Transparent Peer Review report available (PDF)

https://doi.org/10.1021/acs.jpclett.3c02403
J. Phys. Chem. Lett. 2023, 14, 9042−9051

AUTHOR INFORMATION

Corresponding Authors

Eline M. Hutter − *Inorganic Chemistry and Catalysis Group, Debye Institute for Nanomaterials Science and Institute for Sustainable and Circular Chemistry, Department of Chemistry, Utrecht University, 3584 CB Utrecht, The Netherlands;* orcid.org/0000-0002-5537-6545; Email: E.M.Hutter@uu.nl

Loreta A. Muscarella − *Inorganic Chemistry and Catalysis Group, Debye Institute for Nanomaterials Science and Institute for Sustainable and Circular Chemistry, Department of Chemistry, Utrecht University, 3584 CB Utrecht, The Netherlands;* orcid.org/0000-0002-0559-4085; Email: loretaangela.muscarella@gmail.com

Authors

Huygen J. Jöbsis − *Inorganic Chemistry and Catalysis Group, Debye Institute for Nanomaterials Science and Institute for Sustainable and Circular Chemistry, Department of Chemistry, Utrecht University, 3584 CB Utrecht, The Netherlands;* orcid.org/0000-0002-7417-1246

Bettina Baumgartner − *Inorganic Chemistry and Catalysis Group, Debye Institute for Nanomaterials Science and Institute for Sustainable and Circular Chemistry, Department of Chemistry, Utrecht University, 3584 CB Utrecht, The Netherlands;* orcid.org/0000-0002-9136-6811

P. Tim Prins − *Inorganic Chemistry and Catalysis Group, Debye Institute for Nanomaterials Science and Institute for Sustainable and Circular Chemistry, Department of Chemistry, Utrecht University, 3584 CB Utrecht, The Netherlands;* orcid.org/0000-0002-8258-0074

D. Nicolette Maaskant − *Inorganic Chemistry and Catalysis Group, Debye Institute for Nanomaterials Science and Institute for Sustainable and Circular Chemistry, Department of Chemistry, Utrecht University, 3584 CB Utrecht, The Netherlands;* orcid.org/0000-0001-5979-4296

Andrei V. Petukhov − *Physical and Colloid Chemistry, Debye Institute for Nanomaterials Science, Department of Chemistry, Utrecht University, 3584 CH Utrecht, The Netherlands;* orcid.org/0000-0001-9840-6014

Dmitry Chernyshov − *Swiss−Norwegian Beamlines, European Synchrotron Radiation Facility, 38000 Grenoble, France;* orcid.org/0000-0001-7738-9358

Charles J. McMonagle − *Swiss−Norwegian Beamlines, European Synchrotron Radiation Facility, 38000 Grenoble, France*

Complete contact information is available at: https://pubs.acs.org/10.1021/acs.jpclett.3c02403

Author Contributions

‖L.A.M. and H.J.J. contributed equally to this work.

Funding

Open Access is funded by the Austrian Science Fund (FWF).

Notes

The authors declare no competing financial interest.

ACKNOWLEDGMENTS

E.M.H. thanks the Dutch Research Council for funding under Grant VI.Veni.192.034. L.A.M. acknowledges funding from the Dutch Research Council (NWO) under Grant OCENW.XS22.2.039. B.B. acknowledges funding by the Austrian Science Fund (FWF) under Project J4607-N. The authors gratefully acknowledge the European Synchrotron Radiation Facility (ESRF) for the provision of synchrotron radiation beamtime at Swiss-Norwegian beamline BM01 (Proposal MA5378) and Prof. Bert Weckhuysen (Utrecht University) for facilitating the supporting *in situ* XRD measurements. The authors acknowledge funding from the Advanced Research Center Chemical Building Blocks Consortium (ARC CBBC).

REFERENCES

(1) Greul, E.; Petrus, M. L.; Binek, A.; Docampo, P.; Bein, T. Highly Stable, Phase Pure Cs2AgBiBr6 Double Perovskite Thin Films for Optoelectronic Applications. *J. Mater. Chem. A* **2017**, *5* (37), 19972−19981.

(2) Zhang, Z.; Sun, Q.; Lu, Y.; Lu, F.; Mu, X.; Wei, S.; Sui, M. Hydrogenated Cs2AgBiBr6 for Significantly Improved Efficiency of Lead-Free Inorganic Double Perovskite Solar Cell. *Nat. Commun.* **2022**, *13* (13), 3397.

(3) Stranks, S. D.; Eperon, G. E.; Grancini, G.; Menelaou, C.; Alcocer, M. J. P.; Leijtens, T.; Herz, L. M.; Petrozza, A.; Snaith, H. J. Electron-Hole Diffusion Lengths Exceeding 1 Micrometer in an Organometal Trihalide Perovskite Absorber. *Science* **2013**, *342* (6156), 341−344.

(4) Zhang, H.; Ji, X.; Yao, H.; Fan, Q.; Yu, B.; Li, J. Review on Efficiency Improvement Effort of Perovskite Solar Cell. *Sol. Energy* **2022**, *233*, 421−434.

(5) Song, J.; Li, J.; Li, X.; Xu, L.; Dong, Y.; Zeng, H. Quantum Dot Light-Emitting Diodes Based on Inorganic Perovskite Cesium Lead Halides (CsPbX3). *Adv. Mater.* **2015**, *27* (44), 7162−7167.

(6) Yang, D.; Zhao, B.; Yang, T.; Lai, R.; Lan, D.; Friend, R. H.; Di, D. Toward Stable and Efficient Perovskite Light-Emitting Diodes. *Adv. Funct. Mater.* **2022**, *32* (9), 2109495 DOI: 10.1002/adfm.202109495.

(7) Song, X.; Wei, G.; Sun, J.; Peng, C.; Yin, J.; Zhang, X.; Jiang, Y.; Fei, H. Overall Photocatalytic Water Splitting by an Organolead Iodide Crystalline Material. *Nat. Catal.* **2020**, *3*, 1027.

(8) Zhu, X.; Lin, Y.; Sun, Y.; Beard, M. C.; Yan, Y. Lead-Halide Perovskites for Photocatalytic α-Alkylation of Aldehydes. *J. Am. Chem. Soc.* **2019**, *141* (2), 733−738.

(9) Zhang, Z.; Liang, Y.; Huang, H.; Liu, X.; Li, Q.; Chen, L.; Xu, D. Stable and Highly Efficient Photocatalysis with Lead-Free Double-Perovskite of Cs2AgBiBr6. *Angew. Chem. - Int. Ed.* **2019**, *58* (22), 7263−7267.

(10) Jöbsis, H. J.; Fykouras, K.; Reinders, J. W. C.; van Katwijk, J.; Dorresteijn, J. M.; Arens, T.; Vollmer, I.; Muscarella, L. A.; Leppert, L.; Hutter, E. M. Conduction Band Tuning by Controlled Alloying of Fe into $Cs_2AgBiBr_6$ Double Perovskite Powders. *Adv. Funct. Mater.* **2023**, No. 2306106.

(11) Wei, H.; Fang, Y.; Mulligan, P.; Chuirazzi, W.; Fang, H.-H.; Wang, C.; Ecker, B. R.; Gao, Y.; Loi, M. A.; Cao, L.; Huang, J. Sensitive X-Ray Detectors Made of Methylammonium Lead Tribromide Perovskite Single Crystals. *Nat. Photonics* **2016**, *10*, 333−339.

(12) Yakunin, S.; Sytnyk, M.; Kriegner, D.; Shrestha, S.; Richter, M.; Matt, G. J.; Azimi, H.; Brabec, C. J.; Stangl, J.; Kovalenko, M. V.; Heiss, W. Detection of X-Ray Photons by Solution-Processed Lead Halide Perovskites. *Nat. Photonics* **2015**, *9* (7), 444−449.

(13) Steele, J. A.; Pan, W.; Martin, C.; Keshavarz, M.; Debroye, E.; Yuan, H.; Banerjee, S.; Fron, E.; Jonckheere, D.; Kim, C. W.; Baekelant, W.; Niu, G.; Tang, J.; Vanacken, J.; Van der Auweraer, M.; Hofkens, J.; Roeffaers, M. B. J. Photophysical Pathways in Highly Sensitive Cs2AgBiBr6Double-Perovskite Single-Crystal X-Ray Detectors. *Adv. Mater.* **2018**, *30*, 1804450.

(14) Park, B. W.; Philippe, B.; Jain, S. M.; Zhang, X.; Edvinsson, T.; Rensmo, H.; Zietz, B.; Boschloo, G. Chemical Engineering of Methylammonium Lead Iodide/Bromide Perovskites: Tuning of Opto-Electronic Properties and Photovoltaic Performance. *J. Mater. Chem. A* **2015**, *3* (43), 21760−21771.

(15) Du, K.; Meng, W.; Wang, X.; Yan, Y.; Mitzi, D. B. Bandgap Engineering of Lead-Free Double Perovskite Cs2AgBiBr6 through Trivalent Metal Alloying. *Angew. Chem. - Int. Ed.* **2017**, *56* (28), 8158−8162.
(16) Hutter, E. M.; Gélvez-Rueda, M. C.; Bartesaghi, D.; Grozema, F. C.; Savenije, T. J. Band-Like Charge Transport in Cs2AgBiBr6 and Mixed Antimony-Bismuth Cs2AgBi1-XSbxBr6 Halide Double Perovskites. *ACS Omega* **2018**, *3* (9), 11655−11662.
(17) Ji, F.; Wang, F.; Kobera, L.; Abbrent, S.; Brus, J.; Ning, W.; Gao, F. The Atomic-Level Structure of Bandgap Engineered Double Perovskite Alloys Cs2AgIn1−xFexCl6. *Chem. Sci.* **2021**, *12* (5), 1730−1735.
(18) Dakshinamurthy, A. C.; Gupta, M.; Nanda, B. R. K.; Sudakar, C. Anionic Alloying in Hybrid Halide Cs2AgBiBr6- XClxDouble Perovskites: Is It True Alloying or Preferential Occupation of Halide Ions in MX6Octahedra? *J. Phys. Chem. C* **2023**, *127*, 1588.
(19) Gray, M. B.; Mcclure, E. T.; Woodward, P. M. Cs2AgBiBr6-XClx Solid Solutions − Band Gap Engineering with Halide Double Perovskites. *J. Mater. Chem. C* **2019**, *7*, 9686−9689.
(20) Wu, H.; Erbing, A.; Johansson, M. B.; Wang, J.; Kamal, C.; Odelius, M.; Johansson, E. M. J. Mixed-Halide Double Perovskite Cs2AgBiX6 (X = Br, I) with Tunable Optical Properties via Anion Exchange. *ChemSusChem* **2021**, *14* (20), 4507−4515.
(21) Hutter, E. M.; Muscarella, L. A.; Wittmann, F.; Versluis, J.; McGovern, L.; Bakker, H. J.; Woo, Y.-W. W.; Jung, Y.-K. K.; Walsh, A.; Ehrler, B. Thermodynamic Stabilization of Mixed-Halide Perovskites against Phase Segregation. *Cell Reports Phys. Sci.* **2020**, *1* (8), No. 100120.
(22) Muscarella, L. A.; Hutter, E. M.; Wittmann, F.; Woo, Y. W.; Jung, Y.-K.; McGovern, L.; Versluis, J.; Walsh, A.; Bakker, H. J.; Ehrler, B. Lattice Compression Increases the Activation Barrier for Phase Segregation in Mixed-Halide Perovskites. *ACS Energy Lett.* **2020**, *5* (10), 3152−3158.
(23) Jaffe, A.; Lin, Y.; Beavers, C. M.; Voss, J.; Mao, W. L.; Karunadasa, H. I. High-Pressure Single-Crystal Structures of 3D Lead-Halide Hybrid Perovskites and Pressure Effects on Their Electronic and Optical Properties. *ACS Cent. Sci.* **2016**, *2* (4), 201−209.
(24) Zhao, Y.; Miao, P.; Elia, J.; Hu, H.; Wang, X.; Heumueller, T.; Hou, Y.; Matt, G. J.; Osvet, A.; Chen, Y. T.; Tarragó, M.; de Ligny, D.; Przybilla, T.; Denninger, P.; Will, J.; Zhang, J.; Tang, X.; Li, N.; He, C.; Pan, A.; Meixner, A. J.; Spiecker, E.; Zhang, D.; Brabec, C. J. Strain-Activated Light-Induced Halide Segregation in Mixed-Halide Perovskite Solids. *Nat. Commun.* **2020**, *11* (1), 1−9.
(25) Jaffe, A.; Lin, Y.; Karunadasa, H. I. Halide Perovskites under Pressure: Accessing New Properties through Lattice Compression. *ACS Energy Lett.* **2017**, *2* (7), 1549−1555.
(26) Lv, C.; Yang, X.; Shi, Z.; Wang, L.; Sui, L.; Li, Q.; Qin, J.; Liu, K.; Zhang, Z.; Li, X.; Lou, Q.; Yang, D.; Zang, J.; Liu, R.; Liu, B.; Shan, C. X. Pressure-Induced Ultra-Broad-Band Emission of a Cs2AgBiBr6 Perovskite Thin Film. *J. Phys. Chem. C* **2020**, *124* (2), 1732−1738.
(27) Dong, L.; Sun, S.; Deng, Z.; Li, W.; Wei, F.; Qi, Y.; Li, Y.; Li, X.; Lu, P.; Ramamurty, U. Elastic Properties and Thermal Expansion of Lead-Free Halide Double Perovskite Cs2AgBiBr6. *Comput. Mater. Sci.* **2018**, *141*, 49−58.
(28) Girdzis, S. P.; Lin, Y.; Leppert, L.; Slavney, A. H.; Park, S.; Chapman, K. W.; Karunadasa, H. I.; Mao, W. L. Revealing Local Disorder in a Silver-Bismuth Halide Perovskite upon Compression. *J. Phys. Chem. Lett.* **2021**, *12* (1), 532−536.
(29) Zhang, L.; Wang, L.; Wang, K.; Zou, B. Pressure-Induced Structural Evolution and Optical Properties of Metal-Halide Perovskite CsPbCl3. *J. Phys. Chem. C* **2018**, *122* (27), 15220−15225.
(30) Ke, F.; Wang, C.; Jia, C.; Wolf, N. R.; Yan, J.; Niu, S.; Devereaux, T. P.; Karunadasa, H. I.; Mao, W. L.; Lin, Y. Preserving a Robust CsPbI3 Perovskite Phase via Pressure-Directed Octahedral Tilt. *Nat. Commun.* **2021**, *12* (12), 461.
(31) Ghebouli, M. A.; Chihi, T.; Ghebouli, B.; Fatmi, M. Study of the Structural, Elastic, Electronic and Optical Properties of Lead Free Halide Double Perovskites Cs2AgBiX6(X = Br, Cl). *Chin. J. Phys.* **2018**, *56* (1), 323−330.
(32) Xue, D. J.; Hou, Y.; Liu, S. C.; Wei, M.; Chen, B.; Huang, Z.; Li, Z.; Sun, B.; Proppe, A. H.; Dong, Y.; Saidaminov, M. I.; Kelley, S. O.; Hu, J. S.; Sargent, E. H. Regulating Strain in Perovskite Thin Films through Charge-Transport Layers. *Nat. Commun.* **2020**, *11* (1), 1514 DOI: 10.1038/s41467-020-15338-1.
(33) Rodkey, N.; Kaal, S.; Sebastia-Luna, P.; Birkhölzer, Y. A.; Ledinsky, M.; Palazon, F.; Bolink, H. J.; Morales-Masis, M. Pulsed Laser Deposition of Cs2AgBiBr6: From Mechanochemically Synthesized Powders to Dry, Single-Step Deposition. *Chem. Mater.* **2021**, *33* (18), 7417−7422.
(34) Palazon, F.; El Ajjouri, Y.; Bolink, H. J. Making by Grinding: Mechanochemistry Boosts the Development of Halide Perovskites and Other Multinary Metal Halides. *Adv. Energy Mater.* **2020**, *10*, No. 1902499.
(35) Breternitz, J.; Levcenko, S.; Hempel, H.; Gurieva, G.; Franz, A.; Hoser, A.; Schorr, S. Mechanochemical Synthesis of the Lead-Free Double Perovskite Cs2[AgIn]Br6 and Its Optical Properties. *JPhys Energy* **2019**, *1* (2), 025003.
(36) Karmakar, A.; Askar, A. M.; Bernard, G. M.; Terskikh, V. V.; Ha, M.; Patel, S.; Shankar, K.; Michaelis, V. K. Mechanochemical Synthesis of Methylammonium Lead Mixed − Halide Perovskites: Unraveling the Solid-Solution Behavior Using Solid-State NMR. *Chem. Mater.* **2018**, *30*, 2309−2321.
(37) Dyadkin, V.; Pattison, P.; Dmitriev, V.; Chernyshov, D. A New Multipurpose Diffractometer PILATUS@SNBL. *J. Synchrotron Rad.* **2016**, *23*, 825−829.
(38) Rodriguez-Carvajal, J. Recent Advances in Magnetic Structure Determination by Neutron Powder Diffraction. *Phys. Rev. B* **1993**, *192*, 55−69.
(39) Comin, R.; Crawford, M. K.; Said, A. H.; Herron, N.; Guise, W. E.; Wang, X.; Whitfield, P. S.; Jain, A.; Gong, X.; McGaughey, A. J. H.; Sargent, E. H. Lattice Dynamics and the Nature of Structural Transitions in Organolead Halide Perovskites. *Phys. Rev. B* **2016**, *94* (9), No. 094301.
(40) Osherov, A.; Hutter, E. M.; Galkowski, K.; Brenes, R.; Maude, D. K.; Nicholas, R. J.; Plochocka, P.; Bulovic, V.; Savenije, T. J.; Stranks, S. D. The Impact of Phase Retention on the Structural and Optoelectronic Properties of Metal Halide Perovskites. *Adv. Mater.* **2016**, *28*, 10757−10763.
(41) Poglitsch, a.; Weber, D. Dynamic Disorder in Methylammoniumtrihalogenoplumbates (II) Observed by Millimeter-Wave Spectroscopy. *J. Chem. Phys.* **1987**, *87*, 6373.
(42) Lehmann, F.; Franz, A.; Többens, D. M.; Levcenco, S.; Unold, T.; Taubert, A.; Schorr, S. The Phase Diagram of a Mixed Halide (Br, I) Hybrid Perovskite Obtained by Synchrotron X-Ray Diffraction. *RSC Adv.* **2019**, *9* (20), 11151−11159.
(43) Sun, S.; Fang, Y.; Kieslich, G.; White, T. J.; Cheetham, A. K. Mechanical Properties of Organic-Inorganic Halide Perovskites, CH3NH3PbX3 (X = I, Br and Cl), by Nanoindentation. *J. Mater. Chem. A* **2015**, *3* (36), 18450−18455.
(44) Li, C.; Wu, P. Correlation of Bulk Modulus and the Constituent Element Properties of Binary Intermetallic Compounds. *Chem. Mater.* **2001**, *13* (12), 4642−4648.
(45) Saleev, V.; Shipilova, A. Ab Initio Study of Optical and Bulk Properties of Cesium Lead Halide Perovskite Solid Solutions. *Mod. Phys. Lett. B* **2019**, *33*, 1950386.
(46) Min, S.; Choe, H.; Hyun Jung, S.; Cho, J. How Chemical Bonding Impacts Halide Perovskite Nanocrystals Growth to Bulk Films: Implication of Pb−X Bond on Growth Kinetics. *ChemPhysChem* **2023**, DOI: 10.1002/cphc.202300202.
(47) Collings, I. E.; Bykov, M.; Bykova, E.; Hanfland, M.; van Smaalen, S.; Dubrovinsky, L.; Dubrovinskaia, N. Disorder−Order Transitions in the Perovskite Metal− Organic Frameworks [(CH3)-2NH2]IJMIJHCOO)3] at High Pressure. *CrystEngComm* **2018**, *20*, 3512.
(48) Zhou, J.-S.; Alonso, J. A.; Han, J. T.; Fernández-Díaz, M. T.; Cheng, J.-G.; Goodenough, J. B. Jahn−Teller Distortion in Perovskite

KCuF3 under High Pressure. *J. Fluor. Chem.* **2011**, *132* (12), 1117−1121.
(49) Loa, I.; Adler, P.; Grzechnik, A.; Syassen, K.; Schwarz, U.; Hanfland, M.; Rozenberg, G. K.; Gorodetsky, P.; Pasternak, M. P. Pressure-Induced Quenching of the Jahn-Teller Distortion and Insulator-to-Metal Transition in LaMnO3. *Phys. Rev. Lett.* **2001**, *87*, No. 125501.
(50) Ridley, C. J.; Daisenberger, D.; Wilson, C. W.; Stenning, G. B. G.; Sankar, G.; Knight, K. S.; Tucker, M. G.; Smith, R. I.; Bull, C. L. High-Pressure Study of the Elpasolite Perovskite La2NiMnO6. *Inorg. Chem.* **2019**, *58* (14), 9016−9027.
(51) Da Silva, E. L.; Skelton, J. M.; Parker, S. C.; Walsh, A. Phase Stability and Transformations in the Halide Perovskite CsSnI3. *Phys. Rev. B - Condens. Matter Mater. Phys.* **2015**, *91* (14), 1−12.
(52) Dmitriev, V. P.; Chernyshov, D.; Filinchuk, Y. E.; Degtyareva, V. F. Anti-Isostructural Phases and Anomalous Thermoelasticity in In-Based Alloys: Synchrotron x-Ray Diffraction Experiments and Unified Phenomenological Model. *Phys. Rev. B* **2007**, *75*, No. 024111.
(53) Menshikov, A. Z.; Vokhmyanin, A. P.; Dorofeev, Y. A. Magnetic Structure and Phase Transformations in Mn5Si3. *Phys. Status Solidi* **1990**, *158* (1), 319−328.
(54) Van De Goor, T. W. J.; Liu, Y.; Feldmann, S.; Bourelle, S. A.; Neumann, T.; Winkler, T.; Kelly, N. D.; Liu, C.; Jones, M. A.; Emge, S. P.; Friend, R. H.; Monserrat, B.; Deschler, F.; Dutton, S. E. Impact of Orientational Glass Formation and Local Strain on Photo-Induced Halide Segregation in Hybrid Metal-Halide Perovskites. *J. Phys. Chem. C* **2021**, *125* (27), 15025−15034.
(55) Jacobsson, T. J.; Schwan, L. J.; Ottosson, M.; Hagfeldt, A.; Edvinsson, T. Determination of Thermal Expansion Coefficients and Locating the Temperature-Induced Phase Transition in Methylammonium Lead Perovskites Using X-Ray Diffraction. *Inorg. Chem.* **2015**, *54* (22), 10678−10685.
(56) Mu, H.; Zhang, Y.; Zou, H.; Tian, F.; Fu, Y.; Zhang, L. Physical Mechanism and Chemical Trends in the Thermal Expansion of Inorganic Halide Perovskites. *J. Phys. Chem. Lett.* **2023**, *14* (1), 190−198.
(57) Schade, L.; Wright, A. D.; Johnson, R. D.; Dollmann, M.; Wenger, B.; Nayak, P. K.; Prabhakaran, D.; Herz, L. M.; Nicholas, R.; Snaith, H. J.; Radaelli, P. G. Structural and Optical Properties of Cs 2 AgBiBr 6 Double Perovskite. *ACS Energy Lett.* **2019**, *4* (1), 299−305.
(58) Keshavarz, M.; Debroye, E.; Ottesen, M.; Martin, C.; Zhang, H.; Fron, E.; Küchler, R.; Steele, J. A.; Bremholm, M.; Van de Vondel, J.; Wang, H. I.; Bonn, M.; Roeffaers, M. B. J.; Wiedmann, S.; Hofkens, J. Tuning the Structural and Optoelectronic Properties of Cs2AgBiBr6 Double-Perovskite Single Crystals through Alkali-Metal Substitution. *Adv. Mater.* **2020**, *32* (40), 1−10.
(59) Carpenter, M. E.; Salje, E. K. H.; Graeme-Barber, A. Spontaneous Strain as a Determinant of Thermodynamic Properties for Phase Transitions in Minerals. *Eur. J. Mineral.* **1998**, *10*, 621−691.
(60) Keshavarz, M.; Ottesen, M.; Wiedmann, S.; Wharmby, M.; Küchler, R.; Yuan, H.; Debroye, E.; Steele, J. A.; Martens, J.; Hussey, N. E.; Bremholm, M.; Roeffaers, M. B. J.; Hofkens, J. Tracking Structural Phase Transitions in Lead-Halide Perovskites by Means of Thermal Expansion. *Adv. Mater.* **2019**, *31* (24), 1−8.
(61) Heiderhoff, R.; Haeger, T.; Pourdavoud, N.; Hu, T.; Al-Khafaji, M.; Mayer, A.; Chen, Y.; Scheer, H. C.; Riedl, T. Thermal Conductivity of Methylammonium Lead Halide Perovskite Single Crystals and Thin Films: A Comparative Study. *J. Phys. Chem. C* **2017**, *121* (51), 28306−28311.
(62) Haeger, T.; Heiderhoff, R.; Riedl, T. Thermal Properties of Metal-Halide Perovskites. *J. Mater. Chem. C* **2020**, *8* (41), 14289.
(63) Korthuis, V.; Khosrovani, N.; Sleight, A. W.; Roberts, N.; Dupree, R.; Warren, W. W. Negative Thermal Expansion and Phase Transitions in the ZrV2-XPxO7 Series. *Chem. Mater.* **1995**, *7* (2), 412−417.

https://doi.org/10.1021/acs.jpclett.3c02403
J. Phys. Chem. Lett. 2023, 14, 9042−9051